forced shell loaded axisymmetrically. The effect of the eccentricity is certainly transmitted more directly through the tangential component of the interaction load than through the radial component. Thus, it would appear that the eccentricity together with the nonaxisymmetric loading produce a high tensile axial bending stress (at the inner surface) under the load (see Fig. 3).

The radial displacement curve of Fig. 2 reveals that the maximum radial displacement of the shell does not occur under the ring. The reason for behavior of this nature has already been discussed with respect to the bending stresses. The eccentricity of the ring median line with respect to the shell median surface plays a significant role in determining the response of the structure because the tangential component of the interaction line load is of the same order of magnitude as the radial component. We could, therefore, expect substantial changes in the radial displacement pattern as the eccentricity is varied.

It is clear that the experimental and theoretical results agree sufficiently well to corroborate the unanticipated behavior of the loaded structure.

References

[1] Allentuch, A., Brady, K., and Kempner, J., "Long Cylindrical Shell under Concentrated Loads Applied to a Central Reinforcing Ring," *AIAA Journal*, Vol. 5, No. 10, Oct. 1967, pp. 1863–1870; also PIBAL Rept. 680, Dept. of Aerospace Engineering and Applied Mechanics, Polytechnic Inst. of Brooklyn, N. Y.

[2] Donnell, L. J., "Stability of Thin-Walled Tubes under Torsion," Rept. 479, 1934, NACA.

[3] Hoff, N. J., "Boundary Value Problems of the Thin-Walled Circular Cylinder," *Transactions of the ASME: Journal of Applied Mechanics*, Vol. 76, 1954, pp. 343–350.

[4] Pohle, F. V. and Nardo, S. V., "Simplified Formulas for Boundary Value Problems of the Thin-Walled Circular Cylinder," *Journal of Applied Mechanics*, Vol. 22, No. 3, Sept. 1955, pp. 389–390.

[5] Flügge, W., *Stresses in Shells*, Springer-Verlag, Berlin, 1960, pp. 208–218.

Sonic Boom Minimization Including Both Front and Rear Shocks

A. R. George* and R. Seebass*
Cornell University, Ithaca, N. Y.

THE question of whether flights of supersonic aircraft over populated areas will ever be acceptable depends upon the characteristics of the sonic booms of these aircraft. It is not precisely established which characteristics of a sonic boom signature must be reduced to what levels to make a sonic boom acceptable. For observers outdoors it seems sufficient to reduce the shock strengths of the signature below some substantial fraction of one pound per square foot. For observers indoors, however, the magnitude of the impulse of the signature is also of substantial importance.

The problem of aircraft shaping for minimum front shock strengths taking account of midfield effects was treated by the present authors. The present results extend the analysis of Ref. 1 to treat both front and rear shock strengths. The aircraft weight, effective length, and flight conditions are assumed given and lower bounds for shock strengths are found.

Received May 12, 1971; revision received June 11, 1971. This research was sponsored by NASA Grant NGR-33-010-054.

Index category: Aerodynamic and Powerplant Noise (Including Sonic Boom); Supersonic and Hypersonic Flow.

* Associate Professor, Graduate School of Aerospace Engineering.

The first sonic boom optimization analyses were carried out for the asymptotic far field case of an N wave signature by Jones[2] and Carlson.[3] Later McLean[4] pointed out that nonasymptotic effects could be important and Ferri and Ismail[5] demonstrated significant reductions compared to the far field optimums. Jones,[6] George,[1] and Seebass,[7] then independently derived the nonasymptotic optimums minimizing only Δp_F the front shock pressure jump. These analyses did not treat the rear shock strength Δp_R which in some cases can be much stronger than Δp_F. Later Petty[8] included the condition that the magnitude of the perturbation pressure (not Δp_R) in the rear part of the signature satisfy $|p| \leq \Delta p_F$. He found that the minimums were increased somewhat compared to the front shock optimizations. However, his requirement that $|p| \leq \Delta p_F$ restricts Δp_R to be substantially less than Δp_F and results in quite conservative minimums. He also did not allow for the limiting case of rising pressure in the signature as considered in Refs. 1, 6, and 7. A complete review of sonic boom minimization may be found in Ref. 9.

The present work includes the rear shock strength by requiring $\Delta p_R/\Delta p_F = R \leq R_{\max}$. The number $R_{\max}$ was taken as 1.0 in the minimization calculations. Following the development and notation of Ref. 1, the problem can be formulated as finding the Whitham F function shape which minimizes Δp_F with $R \leq R_{\max}$ and holding the lift

$$L = \left(\frac{8q}{\beta}\right)\int_0^a F(y')(a - y')^{1/2}dy' \qquad (1)$$

constant, where a is the aircraft effective length, q the dynamic pressure and $\beta = (M^2 - 1)^{1/2}$. As discussed in Ref. 1 only the case of lift alone will be treated. The shock strengths are found by inserting shock jumps which hold the area under the nonlinearly advanced F curve constant. The perturbation pressure at the ground for flight at altitude r is then given by

$$p = k_r\alpha\gamma p_g M^2(2\beta)^{-1/2}F/r^{1/2}$$

and the normalized nonlinear advance is defined by

$$m = \frac{2^{1/2}\beta^{3/2}}{\tau(\gamma + 1)M^4}\left(\frac{a}{r}\right)^{1/2} = \left(C_T\frac{a_h}{r^{1/2}}\right)^{-1}\frac{(2\beta)^{1/2}}{\gamma M^3}\left(\frac{a}{r}\right)^{1/2}$$

α, τ, and $C_T a_h/r^{1/2}$ are defined in Refs. 1 and 10 and are 1, 1, and $(\gamma + 1)M/\gamma\beta$, respectively for a uniform atmosphere. k_r is the pressure reflection coefficient of the ground.

Using the nondimensional variable $Y = y/a$, the form of the optimum normalized F function is, for $Y \leq 1$,

$$\mathcal{F} = F/a^{1/2}m = K\delta(Y) + C_1H(Y) + JY - (C_1 + C_3 + J)H(Y - Y_C) \qquad (2)$$

where δ and H are unit impulse and step functions, respectively, and K, C_1, C_3, and Y_C are to be determined. This form

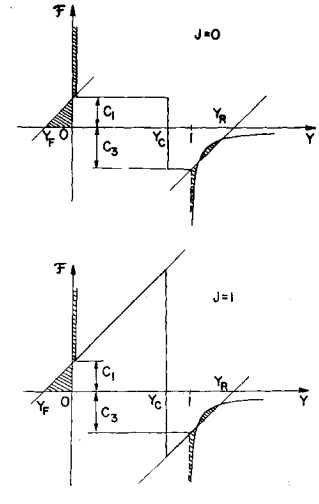

Fig. 1 Optimum $\mathcal{F}$ shapes.

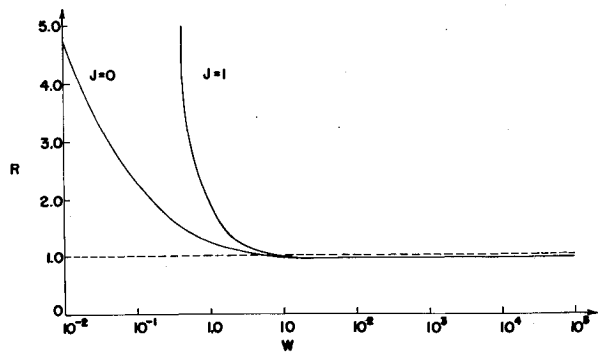

Fig. 2 Ratio of rear to front shock strengths when only Δp_F is minimized.

for $\mathfrak{F}$ is easily shown to minimize both front and rear shocks strengths for the correct choice of Y_C by using the variational analyses presented in Refs. 1, 6, and 8. Examples of these $\mathfrak{F}$ shapes are shown in Fig. 1. The $J = 1$ case gives the minimum shock strength but allows the pressure to rise at the limit of a finite rate after the front shock and before the rear shock. The $J = 0$ case holds p constant in these regions. The shocks are found on the $\mathfrak{F}(Y)$ curves from 45° lines which cut off balanced areas from the $\mathfrak{F}$ curve (shown shaded in the figure). Y_F and Y_R are the as yet unknown values of Y at the most forward and rearward intersections of the shock lines with the $\mathfrak{F}$ curve.

The $\mathfrak{F}$ curve for $Y > 1$ was found from the effective area distributions corresponding to Eq. (2) assuming a constant area wake.† The results for $Y > 1$ are

$$\mathfrak{F}(Y) = (1/\pi)[-K/Y(Y-1)^{1/2} + 2C_1[\sin^{-1}(Y^{-1/2}) - (Y-1)^{-1/2}] + 2J[-(Y-1)^{1/2} + Y\sin^{-1}(Y^{-1/2}) - \tfrac{2}{3}(Y-1)^{-1/2}] - 2(C_1 + C_3 + J)[\sin^{-1}(\{1 - Y_C\}/\{Y - Y_C\})^{1/2} - (\{1 - Y_C\}/\{Y-1\})^{1/2}]] \quad (3)$$

The six unknowns are K, C_1, C_3, Y_F, Y_C, and Y_R, which are to be found from the six conditions: lift given, $\Delta p_R/\Delta p_F = R \leq 1$, front shock area balance, front shock 45° line intersects $\mathfrak{F}$ at Y_F and 0, rear shock area balance, and rear shock 45° line intersects $\mathfrak{F}$ at 1 and Y_R. The nondimensional form of Eq. (1) can be integrated with $\mathfrak{F}$ given by Eq. (2) to give the first condition as

$$W = \beta L/8qa^2m = K + \tfrac{2}{3}C_1 + \tfrac{4}{15}J - \tfrac{2}{3}(C_1 + C_3 + J)(1 - Y_C)^{3/2} \quad (4)$$

The remaining conditions give, successively

$$Y_R - 1 = RY_F \quad (5)$$

$$K = Y_F C_1/2 \quad (6)$$

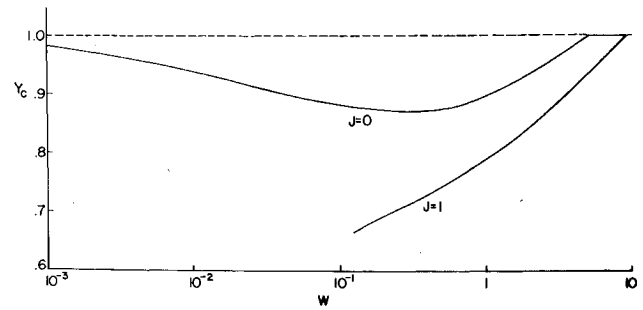

Fig. 3 Y_C for minimum shock strengths vs normalized weight factor.

† The same result can be obtained from Eq. (26) of Ref. 6 or Eq. (6) of Ref. 8.

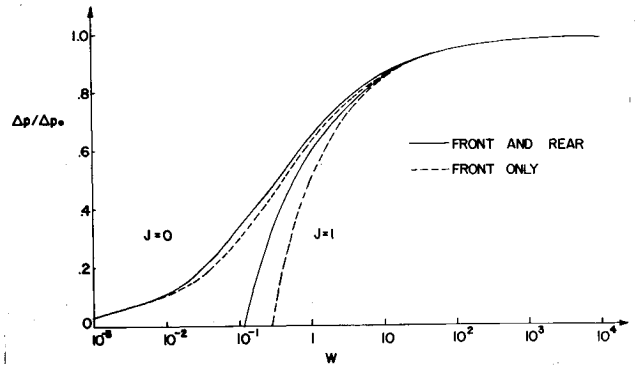

Fig. 4 Shock strength normalized by asymptotic minimum.

$$C_1 = Y_F \quad (7)$$

$$\mathfrak{S}(Y_R) - \mathfrak{S}(1) - [T(Y_R) - T(1)] = 0 \quad (8)$$

where

$$\mathfrak{S}(Y) = \int_0^Y \mathfrak{F}(Y')dY'$$

is a complicated algebraic function and $T(Y) = -(C_3 + 1)Y + Y^2/2$, and finally

$$\mathfrak{F}(Y_R) = C_3 + (Y_R - 1) \quad (9)$$

where $\mathfrak{F}$ is given by Eq. (3). Using Eqs. (4–7), Y_F, Y_R, C_1, and C_3 can be eliminated leaving two algebraic Eqs. (8) and (9) to be numerically solved for K and Y_C whenever the front shock optimizations of Refs. 1, 6, and 7 give $\Delta p_R/\Delta p_F = R > 1$. The minimization of Δp_F alone corresponds to setting $Y_C = 1$ and treating R as unknown. In this case the equations were similarly reduced to the numerical solution of a pair of algebraic equations for C_3 and R.

The results for R for the front shock optimization are shown in Fig. 2. One sees that for higher values of W the Δp_F optimization gives Δp_R slightly less than Δp_F. However, for conditions typical of a commercial SST the value of W is of the order of 0.5, giving large values of R and leading to the present analysis.

The optimum values of Y_C and Δp for $\Delta p_R = \Delta p_F$ were found in the region where $R > 1$ in Fig. 2. The results for Y_C are plotted in Fig. 3. The minimum shock strengths normalized by Δp_0, the asymptotic minimum of Jones,[3] are shown in Fig. 4 along with the values for minimization of the front shock only. It can be seen that for $J = 0$ the values of Y_C are always reasonably near one and the optimum Δp's are only slighter greater than those for Δp_F alone minimized. For low enough W it is seen that Y_C moves back toward one as the tail shock naturally weakens. This effect did not occur in Petty's case where he required $|p| \leq \Delta p_F$. From Fig. 4 it is seen that for $J = 0$ the difference between minimizing both shocks and the front shock alone is never very large, reaching a maximum of 10% of the front only Δp_F for W near 0.1.

For $J = 1$, Y_C asymptotes to $\frac{2}{3}$ at W approximately 0.12 where the signature becomes a "bangless boom" with zero front and rear shock strengths. This concept was introduced by McLean[4] and recently Hayes and Weiskopf[11] reported on some facets of this limit. The present results show that a bangless boom is possible when the nondimensional parameter W is less than approximately 0.12. For W above but near the bangless limit there are large differences between the Δp_F and $\Delta p_R \leq \Delta p_F$ minimizations.

As an example we consider an SST aircraft 300 ft long, weighing 600,000 lb and flying at $M = 3.0$ in the U.S. Standard Atmosphere. For 60,000 ft flight altitude using the results of Ref. 10, one finds $m = 3.63 \times 10^{-3}$ and $W = 0.684$. Then the figures give for $J = 0$, 1, that $Y_C = 0.89$, 0.76 and

$\Delta p/\Delta p_0 = 0.605, 0.528$. This results in Δp's of 1.64, 0.996, and 0.870 psf for the asymptotic, constant overpressure, and rising pressure cases. For comparison minimizing the front shock only would give $\Delta p_F = 0.958$ and 0.645 psf for $J = 0$, 1. Thus as was already evident from the discussion, only the $J = 1$ case differs significantly from the Δp_F only optimization. If the flight altitude is decreased to 40,000 ft, m becomes 4.68×10^{-3} and $W = 0.203$. In this case the Δp's are 2.26, 0.967, and 0.464 psf for the asymptotic, $J = 0$ and $J = 1$ cases. Thus, as previously pointed out in Ref. 1, the use of midfield optimizations can nearly eliminate the effect of increased flight altitude. This allows lower flight altitudes with comparable or reduced sonic boom strengths. A bangless boom can be obtained for 40,000 ft altitude if the present 300 ft aircraft weighs less than 355,000 lb. This weight, although stringent, is not beyond the realm of possibility.

As discussed in Refs. 1 and 2, the effective cross-sectional areas required for these shapes are not extreme and the present shapes are more easily approached than the asymptotic case. The discontinuity in $\bar{s}$ at Y_C requires only a $(Y - Y_C)^{3/2}$ or $(Y - Y_C)^{1/2}$ effective area or lift distribution, respectively, and should be easy to approximate in a real design.

References

[1] George, A. R., "Lower Bounds for Sonic Booms in the Midfield," *AIAA Journal*, Vol. 7, No. 8, Aug. 1969, pp. 1542–1545.

[2] Jones, L. B., "Lower Bounds for Sonic Bangs," *Journal of the Royal Aeronautical Society*, Vol. 65, June 1961, pp. 433–436; also "Lower Bounds for Sonic Bangs in the Far Field," *Aeronautical Quarterly*, Vol. 18, Pt. 1, Feb. 1967, pp. 1–21.

[3] Carlson, H. W., "The Lower Bound of Attainable Sonic-Boom Overpressure and Design Methods of Approaching this Limit," TN D-1494, Oct. 1962, NASA.

[4] McLean, F. E., "Some Nonasymptotic Effects on the Sonic Boom of Large Airplanes," TN D-2877, June 1965, NASA.

[5] Ferri, A. and Ismail, A., "Report on Sonic Boom Studies, Pt. 1, Analysis of Configurations," *Second Conference on Sonic Boom Research*, edited by I. R. Schwartz, NASA SP-180, 1968, pp. 73–88.

[6] Jones, L. B., "Lower Bounds for the Pressure Jump of the Bow Shock of a Supersonic Transport," *Aeronautical Quarterly*, Vol. 21, Feb. 1970, pp. 1–17.

[7] Seebass, R., "Sonic Boom Theory," *Journal of Aircraft*, Vol. 6, No. 3, May-June, 1969, pp. 177–184.

[8] Petty, J. S., "Lower Bounds for Sonic Boom Considering the Negative Overpressure Region," *Journal of Aircraft*, Vol. 7, No. 4, July-Aug. 1970, pp. 375–377.

[9] Sebass, R. and George, A. R., "Sonic Boom Minimization," *Journal of the Acoustical Society of America*, to be published.

[10] George, A. R. and Plotkin, K. J., "Sonic Boom Waveforms and Amplitudes in a Real Atmosphere," *AIAA Journal*, Vol. 7, No. 10, Oct. 1969, pp. 1978–1981.

[11] Hayes, W. D., Gardner, J. H., Caughey, D. A., and Weiskopf, F. B., Jr., "Theoretical Problems Related to Sonic Boom," *Third Conference on Sonic Boom Research*, edited by I. R. Schwartz, NASA SP-255, 1971, pp. 27–31.

Delta Wing Shock Shape at Hypersonic Speed

DHANVADA MADHAVA RAO*

NASA Langley Research Center, Hampton, Va.

THE considerable literature on delta wing hypersonic aerodynamics offers little information on the three-dimensional shock shape. The situation appears anomalous in view of the fact that the shock shape is the starting point and the controlling feature in many theoretical solutions of the delta wing flowfield. The ability to calculate the shock envelope is of practical importance when, for example, the effects of possible interaction with other vehicle components are considered, which can lead to serious heating, stability, and control problems.

Received May 24, 1971.

* Resident Research Associate, Configuration Flow Fields Section, Hypersonic Vehicles Division; on leave from National Aeronautical Laboratory, Bangalore, India. Member AIAA.

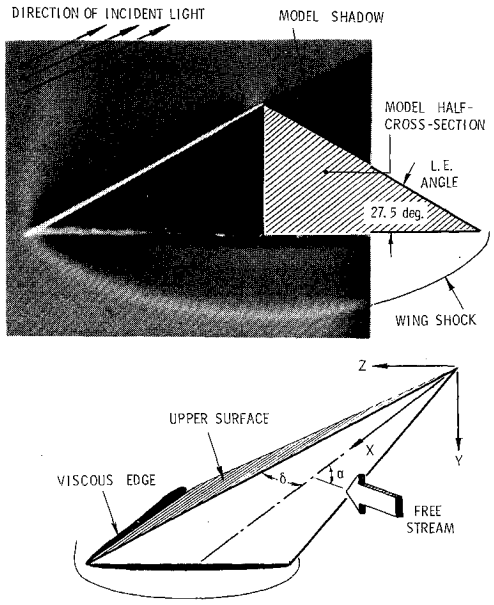

Fig. 1 Typical vapor screen photograph ($\alpha = 13°$); coordinate system and angles.

Experimentally, the determination of the three-dimensional shock surface is usually a tedious point-by-point procedure involving pitot-tube traversing of the flowfield. During a recent program of flow-visualization tests on delta wings using the vapor screen method (commonly employed for qualitative flowfield studies in wind tunnels) good quality photographs were obtained in which the entire shock envelope cross section was clearly visible (see Fig. 1). This suggested the use of the vapor screen technique as a rapid means of determining the shock envelope of complex shapes. However, due to unknown aerodynamic effects in a condensing flow, the quantitative validity of the method has first to be established.

The present Note is concerned with an exploratory evaluation of the above idea. A comparison of the shock measurements with schlieren results as well as with theoretical calculations by the method of Squire[1] has been made. The cases studied herein correspond to shocks detached from the leading edges, a condition typical of hypersonic flight.

A flat-bottom delta wing model with "roof-top" and sharp leading-edges swept back at 75° was tested in the Langley 11-in. Blowdown Tunnel fitted with a two-dimensional $M = 6.8$ nozzle, using dry air. The tunnel was run "cold," i.e., at ambient stagnation temperature, to permit a partial condensation in the flow.† The freestream Reynolds number was approximately 0.4 million per in., giving a model length Reynolds number of nearly 4 million. The vapor screen was formed by illuminating a thin slice (0.1 in.) of the flow normal to the freestream and the bottom surface of the model, positioned about 1 in. upstream of the trailing-edge. Flowfield photographs were taken at incidence angle of the lower surface $\alpha = 8°, 13°$, and 18°.

Schlieren photographs were obtained in subsequent hot-flow runs repeated at the same incidence angles (with model Reynolds number of about 4.5 million). This provided center-plane shock data for comparison with the vapor screen results and, as seen in Fig. 2, excellent agreement is found.

† It may be noted that while at lower Mach numbers the vapor screen depends on a two-phase flow containing water vapor, in this case the liquefaction of oxygen, or even a three-phase flow with solid carbon dioxide particles, is likely to occur.